

Observation of $B^+ \rightarrow K_1(1270)^+ \gamma$

K. Abe,¹⁰ K. Abe,⁴⁶ N. Abe,⁴⁹ I. Adachi,¹⁰ H. Aihara,⁴⁸ M. Akatsu,²⁴ Y. Asano,⁵³
T. Aso,⁵² V. Aulchenko,² T. Aushev,¹⁴ T. Aziz,⁴⁴ S. Bahinipati,⁶ A. M. Bakich,⁴³
Y. Ban,³⁶ M. Barbero,⁹ A. Bay,²⁰ I. Bedny,² U. Bitenc,¹⁵ I. Bizjak,¹⁵ S. Blyth,²⁹
A. Bondar,² A. Bozek,³⁰ M. Bračko,^{22,15} J. Brodzicka,³⁰ T. E. Browder,⁹ M.-C. Chang,²⁹
P. Chang,²⁹ Y. Chao,²⁹ A. Chen,²⁶ K.-F. Chen,²⁹ W. T. Chen,²⁶ B. G. Cheon,⁴
R. Chistov,¹⁴ S.-K. Choi,⁸ Y. Choi,⁴² Y. K. Choi,⁴² A. Chuvikov,³⁷ S. Cole,⁴³
M. Danilov,¹⁴ M. Dash,⁵⁵ L. Y. Dong,¹² R. Dowd,²³ J. Dragic,²³ A. Drutskoy,⁶
S. Eidelman,² Y. Enari,²⁴ D. Epifanov,² C. W. Everton,²³ F. Fang,⁹ S. Fratina,¹⁵
H. Fujii,¹⁰ N. Gabyshev,² A. Garmash,³⁷ T. Gershon,¹⁰ A. Go,²⁶ G. Gokhroo,⁴⁴
B. Golob,^{21,15} M. Grosse Perdekamp,³⁸ H. Guler,⁹ J. Haba,¹⁰ F. Handa,⁴⁷ K. Hara,¹⁰
T. Hara,³⁴ N. C. Hastings,¹⁰ K. Hasuko,³⁸ K. Hayasaka,²⁴ H. Hayashii,²⁵ M. Hazumi,¹⁰
E. M. Heenan,²³ I. Higuchi,⁴⁷ T. Higuchi,¹⁰ L. Hinz,²⁰ T. Hojo,³⁴ T. Hokuue,²⁴
Y. Hoshi,⁴⁶ K. Hoshina,⁵¹ S. Hou,²⁶ W.-S. Hou,²⁹ Y. B. Hsiung,²⁹ H.-C. Huang,²⁹
T. Igaki,²⁴ Y. Igarashi,¹⁰ T. Iijima,²⁴ A. Imoto,²⁵ K. Inami,²⁴ A. Ishikawa,¹⁰ H. Ishino,⁴⁹
K. Itoh,⁴⁸ R. Itoh,¹⁰ M. Iwamoto,³ M. Iwasaki,⁴⁸ Y. Iwasaki,¹⁰ R. Kagan,¹⁴ H. Kakuno,⁴⁸
J. H. Kang,⁵⁶ J. S. Kang,¹⁷ P. Kapusta,³⁰ S. U. Kataoka,²⁵ N. Katayama,¹⁰ H. Kawai,³
H. Kawai,⁴⁸ Y. Kawakami,²⁴ N. Kawamura,¹ T. Kawasaki,³² N. Kent,⁹ H. R. Khan,⁴⁹
A. Kibayashi,⁴⁹ H. Kichimi,¹⁰ H. J. Kim,¹⁹ H. O. Kim,⁴² Hyunwoo Kim,¹⁷ J. H. Kim,⁴²
S. K. Kim,⁴¹ T. H. Kim,⁵⁶ K. Kinoshita,⁶ P. Koppenburg,¹⁰ S. Korpar,^{22,15} P. Križan,^{21,15}
P. Krokovny,² R. Kulasiri,⁶ C. C. Kuo,²⁶ H. Kurashiro,⁴⁹ E. Kurihara,³ A. Kusaka,⁴⁸
A. Kuzmin,² Y.-J. Kwon,⁵⁶ J. S. Lange,⁷ G. Leder,¹³ S. E. Lee,⁴¹ S. H. Lee,⁴¹
Y.-J. Lee,²⁹ T. Lesiak,³⁰ J. Li,⁴⁰ A. Limosani,²³ S.-W. Lin,²⁹ D. Liventsev,¹⁴
J. MacNaughton,¹³ G. Majumder,⁴⁴ F. Mandl,¹³ D. Marlow,³⁷ T. Matsuishi,²⁴
H. Matsumoto,³² S. Matsumoto,⁵ T. Matsumoto,⁵⁰ A. Matyja,³⁰ Y. Mikami,⁴⁷
W. Mitaroff,¹³ K. Miyabayashi,²⁵ Y. Miyabayashi,²⁴ H. Miyake,³⁴ H. Miyata,³² R. Mizuk,¹⁴
D. Mohapatra,⁵⁵ G. R. Moloney,²³ G. F. Moorhead,²³ T. Mori,⁴⁹ A. Murakami,³⁹
T. Nagamine,⁴⁷ Y. Nagasaka,¹¹ T. Nakadaira,⁴⁸ I. Nakamura,¹⁰ E. Nakano,³³ M. Nakao,¹⁰
H. Nakazawa,¹⁰ Z. Natkaniec,³⁰ K. Neichi,⁴⁶ S. Nishida,¹⁰ O. Nitoh,⁵¹ S. Noguchi,²⁵
T. Nozaki,¹⁰ A. Ogawa,³⁸ S. Ogawa,⁴⁵ T. Ohshima,²⁴ T. Okabe,²⁴ S. Okuno,¹⁶
S. L. Olsen,⁹ Y. Onuki,³² W. Ostrowicz,³⁰ H. Ozaki,¹⁰ P. Pakhlov,¹⁴ H. Palka,³⁰
C. W. Park,⁴² H. Park,¹⁹ K. S. Park,⁴² N. Parslow,⁴³ L. S. Peak,⁴³ M. Pernicka,¹³
J.-P. Perroud,²⁰ M. Peters,⁹ L. E. Piilonen,⁵⁵ A. Poluektov,² F. J. Ronga,¹⁰ N. Root,²
M. Rozanska,³⁰ H. Sagawa,¹⁰ M. Saigo,⁴⁷ S. Saitoh,¹⁰ Y. Sakai,¹⁰ H. Sakamoto,¹⁸
T. R. Sarangi,¹⁰ M. Satapathy,⁵⁴ N. Sato,²⁴ O. Schneider,²⁰ J. Schümann,²⁹ C. Schwanda,¹³
A. J. Schwartz,⁶ T. Seki,⁵⁰ S. Semenov,¹⁴ K. Senyo,²⁴ Y. Settai,⁵ R. Seuster,⁹
M. E. Sevier,²³ T. Shibata,³² H. Shibuya,⁴⁵ B. Shwartz,² V. Sidorov,² V. Siegle,³⁸
J. B. Singh,³⁵ A. Somov,⁶ N. Soni,³⁵ R. Stamen,¹⁰ S. Stanič,^{53,*} M. Starič,¹⁵ A. Sugi,²⁴
A. Sugiyama,³⁹ K. Sumisawa,³⁴ T. Sumiyoshi,⁵⁰ S. Suzuki,³⁹ S. Y. Suzuki,¹⁰ O. Tajima,¹⁰
F. Takasaki,¹⁰ K. Tamai,¹⁰ N. Tamura,³² K. Tanabe,⁴⁸ M. Tanaka,¹⁰ G. N. Taylor,²³
Y. Teramoto,³³ X. C. Tian,³⁶ S. Tokuda,²⁴ S. N. Tovey,²³ K. Trabelsi,⁹ T. Tsuboyama,¹⁰

T. Tsukamoto,¹⁰ K. Uchida,⁹ S. Uehara,¹⁰ T. Uglov,¹⁴ K. Ueno,²⁹ Y. Unno,³ S. Uno,¹⁰
Y. Ushiroda,¹⁰ G. Varner,⁹ K. E. Varvell,⁴³ S. Villa,²⁰ C. C. Wang,²⁹ C. H. Wang,²⁸
J. G. Wang,⁵⁵ M.-Z. Wang,²⁹ M. Watanabe,³² Y. Watanabe,⁴⁹ L. Widhalm,¹³
Q. L. Xie,¹² B. D. Yabsley,⁵⁵ A. Yamaguchi,⁴⁷ H. Yamamoto,⁴⁷ S. Yamamoto,⁵⁰
T. Yamanaka,³⁴ Y. Yamashita,³¹ M. Yamauchi,¹⁰ Heyoung Yang,⁴¹ P. Yeh,²⁹ J. Ying,³⁶
K. Yoshida,²⁴ Y. Yuan,¹² Y. Yusa,⁴⁷ H. Yuta,¹ S. L. Zang,¹² C. C. Zhang,¹² J. Zhang,¹⁰
L. M. Zhang,⁴⁰ Z. P. Zhang,⁴⁰ V. Zhilich,² T. Ziegler,³⁷ D. Žontar,^{21, 15} and D. Zürcher²⁰

(The Belle Collaboration)

¹*Aomori University, Aomori*

²*Budker Institute of Nuclear Physics, Novosibirsk*

³*Chiba University, Chiba*

⁴*Chonnam National University, Kwangju*

⁵*Chuo University, Tokyo*

⁶*University of Cincinnati, Cincinnati, Ohio 45221*

⁷*University of Frankfurt, Frankfurt*

⁸*Gyeongsang National University, Chinju*

⁹*University of Hawaii, Honolulu, Hawaii 96822*

¹⁰*High Energy Accelerator Research Organization (KEK), Tsukuba*

¹¹*Hiroshima Institute of Technology, Hiroshima*

¹²*Institute of High Energy Physics,*

Chinese Academy of Sciences, Beijing

¹³*Institute of High Energy Physics, Vienna*

¹⁴*Institute for Theoretical and Experimental Physics, Moscow*

¹⁵*J. Stefan Institute, Ljubljana*

¹⁶*Kanagawa University, Yokohama*

¹⁷*Korea University, Seoul*

¹⁸*Kyoto University, Kyoto*

¹⁹*Kyungpook National University, Taegu*

²⁰*Swiss Federal Institute of Technology of Lausanne, EPFL, Lausanne*

²¹*University of Ljubljana, Ljubljana*

²²*University of Maribor, Maribor*

²³*University of Melbourne, Victoria*

²⁴*Nagoya University, Nagoya*

²⁵*Nara Women's University, Nara*

²⁶*National Central University, Chung-li*

²⁷*National Kaohsiung Normal University, Kaohsiung*

²⁸*National United University, Miao Li*

²⁹*Department of Physics, National Taiwan University, Taipei*

³⁰*H. Niewodniczanski Institute of Nuclear Physics, Krakow*

³¹*Nihon Dental College, Niigata*

³²*Niigata University, Niigata*

³³*Osaka City University, Osaka*

³⁴*Osaka University, Osaka*

³⁵*Panjab University, Chandigarh*

³⁶*Peking University, Beijing*

³⁷*Princeton University, Princeton, New Jersey 08545*

³⁸*RIKEN BNL Research Center, Upton, New York 11973*

³⁹*Saga University, Saga*

⁴⁰*University of Science and Technology of China, Hefei*

⁴¹*Seoul National University, Seoul*

⁴²*Sungkyunkwan University, Suwon*

⁴³*University of Sydney, Sydney NSW*

⁴⁴*Tata Institute of Fundamental Research, Bombay*

⁴⁵*Toho University, Funabashi*

⁴⁶*Tohoku Gakuin University, Tagajo*

⁴⁷*Tohoku University, Sendai*

⁴⁸*Department of Physics, University of Tokyo, Tokyo*

⁴⁹*Tokyo Institute of Technology, Tokyo*

⁵⁰*Tokyo Metropolitan University, Tokyo*

⁵¹*Tokyo University of Agriculture and Technology, Tokyo*

⁵²*Toyama National College of Maritime Technology, Toyama*

⁵³*University of Tsukuba, Tsukuba*

⁵⁴*Utkal University, Bhubaneswer*

⁵⁵*Virginia Polytechnic Institute and State University, Blacksburg, Virginia 24061*

⁵⁶*Yonsei University, Seoul*

Abstract

We report the observation of the radiative decay $B^+ \rightarrow K_1(1270)^+\gamma$ using a data sample of 140 fb^{-1} taken at the $\Upsilon(4S)$ resonance with the Belle detector at the KEKB e^+e^- collider. We find the branching fraction to be $\mathcal{B}(B^+ \rightarrow K_1(1270)^+\gamma) = (4.28 \pm 0.94(\text{stat.}) \pm 0.43(\text{syst.})) \times 10^{-5}$ with a statistical significance of 9.2σ . We find no significant signal for $B^+ \rightarrow K_1(1400)^+\gamma$ and set an upper limit $\mathcal{B}(B^+ \rightarrow K_1(1400)^+\gamma) < 1.44 \times 10^{-5}$ at the 90% confidence level. We also measure inclusive branching fractions for $B^+ \rightarrow K^+\pi^+\pi^-\gamma$ and $B^0 \rightarrow K^0\pi^+\pi^-\gamma$ in the mass range $1 \text{ GeV}/c^2 < M_{K\pi\pi} < 2 \text{ GeV}/c^2$.

PACS numbers: 13.25.Hw, 14.40.Nd

Radiative B decays that occur through the flavor changing neutral current process $b \rightarrow s\gamma$ have been one of the most sensitive probes to search for physics beyond the Standard Model (SM). The first observed exclusive radiative decay mode was $B \rightarrow K^*\gamma$ [1, 2], which accounts for around 15% of the total $b \rightarrow s\gamma$ branching fraction. The second mode was $B \rightarrow K_2^*(1430)\gamma$, for which evidence was reported by CLEO and Belle [1, 3]. No other exclusive radiative decay mode into a two-body final state has been reported; for multi-body final states, Belle has observed $B^+ \rightarrow K^+\pi^+\pi^-\gamma$ [4] which is almost saturated by $K^{*0}\pi^+\gamma$ and $K^+\rho^0\gamma$ using a 29 fb^{-1} data sample [3], and $B^+ \rightarrow K^+\phi\gamma$ using 90 fb^{-1} [5].

According to theoretical predictions [6, 7], the branching fraction of unobserved modes among such exclusive decays should be within the current experimental sensitivity. Some of these two-body decay modes are particularly interesting. For example, $B \rightarrow K_1(1270)\gamma$ and $B \rightarrow K_1(1400)\gamma$ ($K_1 \rightarrow K\pi\pi$) can be used to measure the photon helicity, which may differ from the SM prediction in some models beyond the SM [8]. The neutral decay mode $B^0 \rightarrow K_1(1270)^0\gamma$, $K_1(1270)^0 \rightarrow K_S^0\rho^0$ would be a useful channel to measure time-dependent CP violation, which is also sensitive to the photon helicity in radiative B decay.

In this paper, we report the observation of $B^+ \rightarrow K_1(1270)^+\gamma$, which is the first radiative B meson decay mode that involves an axial-vector resonance. We study radiative decays in the $K^+\pi^+\pi^-\gamma$ and $K_S^0\pi^+\pi^-\gamma$ final states, where we search for resonant structure in the $K^+\pi^+\pi^-$ system. We also report inclusive measurements of $B^+ \rightarrow K^+\pi^+\pi^-\gamma$ and $B^0 \rightarrow K^0\pi^+\pi^-\gamma$, and the results of a search for $B^+ \rightarrow K_1(1400)^+\gamma$. The analysis is based on a data sample of 140 fb^{-1} taken at the $\Upsilon(4S)$ resonance with the Belle detector at the KEKB e^+e^- collider [9]. The data sample contains 152 million $B\bar{B}$ pairs.

The Belle detector is a large-solid-angle magnetic spectrometer that consists of a three-layer silicon vertex detector (SVD), a 50-layer central drift chamber (CDC), an array of aerogel threshold Čerenkov counters (ACC), a barrel-like arrangement of time-of-flight scintillation counters (TOF), and an electromagnetic calorimeter comprised of CsI(Tl) crystals (ECL) located inside a super-conducting solenoid coil that provides a 1.5 T magnetic field. An iron flux-return located outside of the coil is instrumented to detect K_L^0 mesons and to identify muons (KLM). The detector is described in detail elsewhere [10].

The photon candidate is the highest energy photon cluster measured with the barrel ECL ($33^\circ < \theta_\gamma < 128^\circ$ in the laboratory frame) and is required to be an isolated electromagnetic shower, i.e. 95% of its energy be concentrated in an array of central 3×3 crystals out of 5×5 crystals and the shower width be less than 5 cm. In order to reduce the background due to photons from π^0 and η decays, we combine the photon candidate with all other photon clusters in the event with the energy greater than 30 MeV (200 MeV) and reject the event if the invariant mass of any pair is within $\pm 18\text{ MeV}/c^2$ ($\pm 32\text{ MeV}/c^2$) around the nominal π^0 (η) mass. We refer to this requirement as the π^0/η veto.

Charged tracks, that are reconstructed with the CDC and SVD, are required to have the momentum in the center-of-mass (c.m.) frame greater than $200\text{ MeV}/c$ and to have an impact parameter relative to the interaction point of less than 5 cm along the positron beam axis and less than 0.5 cm in the plane that is transverse to this axis. These tracks are identified as pion or kaon candidates by a likelihood ratio based on the combined information from the ACC and TOF systems and the dE/dx measurement in the CDC. We require the kaon likelihood ratio larger than 0.6 for kaons; the remaining tracks are considered as pion candidates. In addition, we remove kaon and pion candidates if they are identified as an electron, muon or proton.

For neutral kaons, we use $K_S^0 \rightarrow \pi^+\pi^-$ candidates that have invariant masses within

$\pm 30 \text{ MeV}/c^2$ of the K_S^0 mass and have the c.m. momentum greater than $200 \text{ MeV}/c$. We do not apply the particle identification criteria for these pions. The two pions are required to have a common vertex that is displaced from the interaction point. The K_S^0 momentum direction is also required to be consistent with the K_S^0 flight direction.

We select $K^+\pi^+\pi^-$ and $K_S^0\pi^+\pi^-$ combinations in the mass range $1 \text{ GeV}/c^2 < M_{K\pi\pi} < 2 \text{ GeV}/c^2$. We combine this $K\pi^+\pi^-$ system and the photon candidate, and identify B meson candidates using the following two independent kinematic variables: the beam-energy constrained mass $M_{bc} \equiv \sqrt{(E_{\text{beam}}^*/c^2)^2 - |\vec{p}_B^*/c|^2}$ and the energy difference $\Delta E \equiv E_{K\pi\pi}^* + E_\gamma^* - E_{\text{beam}}^*$, where E_{beam}^* is the beam energy and \vec{p}_B^* is the momentum of the B candidate in the c.m. frame. (Variables with an asterisk are calculated in the c.m. frame.) The momentum \vec{p}_B^* is calculated without using the absolute value of the photon momentum according to

$$\vec{p}_B^* = \vec{p}_{K\pi\pi}^* + \frac{\vec{p}_\gamma^*}{E_\gamma^*} \times (E_{\text{beam}}^* - E_{K\pi\pi}^*) \quad (1)$$

since the $K\pi^+\pi^-$ momentum $\vec{p}_{K\pi\pi}^*$ and the beam energy are determined with substantially better precision than that of the primary photon.

We select B candidates within $-0.1 \text{ GeV} < \Delta E < 0.08 \text{ GeV}$ and $M_{bc} > 5.2 \text{ GeV}/c^2$. If there exist multiple candidates, we choose the candidate that has the highest confidence level for the $K^+\pi^+\pi^-$ ($\pi^+\pi^-$ for the $K_S^0\pi^+\pi^-$ mode) vertex fit.

The continuum background ($e^+e^- \rightarrow q\bar{q}$, $q = u, d, s, c$) is the dominant background in this analysis. To separate signal events from continuum background events, we use two variables: the B flight direction ($\cos\theta_B$) and a Fisher discriminant [11] constructed from a set of shape variables [12]. We determine the probability density functions for signal and continuum background for each of these variables, and combine them into a likelihood ratio.

The $\cos\theta_B$ distribution of the signal events follows a $1 - \cos^2\theta_B$ distribution while that of $q\bar{q}$ has a nearly uniform distribution. The likelihood function for the flight direction $\mathcal{L}_{S(B)}^{\cos\theta_B}$ is modeled as a second (first) order polynomial of $\cos\theta_B$ for the signal (continuum background).

For the shape variables, we use 16 modified Fox-Wolfram moments [12, 13] that are calculated from the particle momenta in the following four categories: 1) particles that form the signal candidate, 2) the remaining charged particles, 3) the remaining neutral particles, and 4) a hypothetical particle for the missing momentum of the event. The Fisher discriminant is calculated from these moments and the scalar sum of the transverse momentum. The likelihood function for this Fisher discriminant $\mathcal{L}_{S(B)}^{\text{Fisher}}$ is modeled by a bifurcated Gaussian function both for the signal and for the continuum background.

These likelihood functions are then combined using a single likelihood ratio,

$$\mathcal{R}_S = \frac{\mathcal{L}_S^{\cos\theta_B} \mathcal{L}_S^{\text{Fisher}}}{\mathcal{L}_S^{\cos\theta_B} \mathcal{L}_S^{\text{Fisher}} + \mathcal{L}_B^{\cos\theta_B} \mathcal{L}_B^{\text{Fisher}}} \quad (2)$$

We determine the \mathcal{R}_S requirement by maximizing $N_S / \sqrt{N_S + N_B}$, where N_S and N_B are the expected number of the signal and background events, respectively. For this purpose, we use four signal Monte Carlo (MC) samples, $B^+ \rightarrow K_1(1270)^+\gamma$ and $B^0 \rightarrow K_1(1270)^0\gamma$ in the $K\pi^+\pi^-$ mass range $1.1 \text{ GeV}/c^2 < M_{K\pi\pi} < 1.5 \text{ GeV}/c^2$, and $B^+ \rightarrow K_1(1400)^+\gamma$ and $B^0 \rightarrow K_1(1400)^0\gamma$ in $1.225 \text{ GeV}/c^2 < M_{K\pi\pi} < 1.575 \text{ GeV}/c^2$, assuming all the $B \rightarrow K_1\gamma$ branching fractions are 1×10^{-5} . We find a requirement of $\mathcal{R}_S > 0.9$ is optimal for all four cases.

The signal yields for $B^+ \rightarrow K^+\pi^+\pi^-\gamma$ and $B^0 \rightarrow K^0\pi^+\pi^-\gamma$ are extracted from a binned maximum likelihood fit to the M_{bc} distribution with signal and background components. In addition to the continuum background, we consider four B decay background sources: a collection of known B decays through the $b \rightarrow c$ transition (referred to as the $b \rightarrow c$ background), hadronic B decays through the $b \rightarrow u$, $b \rightarrow s$ and $b \rightarrow d$ transitions (charmless background), $B \rightarrow K^*\gamma$ background, and radiative decays to the final states other than $K^*\gamma$ and $K\pi^+\pi^-\gamma$ (other $b \rightarrow s\gamma$ background). In order to suppress the $B \rightarrow K^*\gamma$ background, we reject the event if ΔE and M_{bc} calculated from the $K\pi\gamma$ combination is within $-0.2 \text{ GeV} < \Delta E < 0.1 \text{ GeV}$ and $M_{bc} > 5.27 \text{ GeV}/c^2$.

The signal M_{bc} distribution is modeled with a single Gaussian function at the B meson mass with a resolution of $2.6 \text{ MeV}/c^2$, that is calibrated using a $B^0 \rightarrow D^-\pi^+$, $D^- \rightarrow K^+\pi^-\pi^-$ ($B^+ \rightarrow \bar{D}^0\pi^+$, $\bar{D}^0 \rightarrow K_S^0\pi^+\pi^-$) sample for the $K^+\pi^+\pi^-\gamma$ ($K_S^0\pi^+\pi^-\gamma$) final state. We model the background M_{bc} distributions using large samples of MC events. We find the sum of the continuum and $b \rightarrow c$ backgrounds is described by an ARGUS function [14]. The ARGUS shape parameter is taken from the MC sample, which is consistent with the ΔE sideband data in $0.1 \text{ GeV} < \Delta E < 0.2 \text{ GeV}$ where B decay backgrounds are negligible. Charmless decays, $B \rightarrow K^*\gamma$ and other $b \rightarrow s\gamma$ decays each produce a small signal-like component on top of the background-like component. We model each of these backgrounds as a sum of an ARGUS function and a Gaussian function. The size of the continuum plus $b \rightarrow c$ background is floated in the fit; the size of the other three components are fixed in the fit.

The fit result is shown in Fig. 1. For the $B^+ \rightarrow K^+\pi^+\pi^-\gamma$ mode, we obtain 318 ± 22 events with a statistical significance of 20.4σ , where the significance is defined as $\sqrt{-2 \ln(\mathcal{L}_0/\mathcal{L}_{\max})}$, and \mathcal{L}_{\max} and \mathcal{L}_0 denote the maximum likelihoods of the fit with and without the signal component, respectively. Similarly, we obtain 67 ± 10 events with a statistical significance of 10.9σ for the $B^0 \rightarrow K^0\pi^+\pi^-\gamma$ mode.

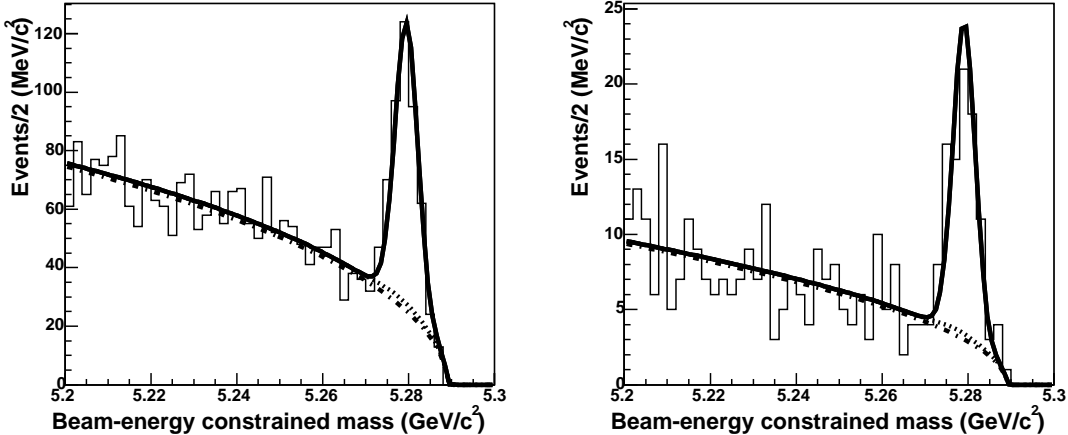


FIG. 1: M_{bc} distributions for $B^+ \rightarrow K^+\pi^+\pi^-\gamma$ (left) and $B^0 \rightarrow K^0\pi^+\pi^-\gamma$ (right). Lines show the continuum plus $b \rightarrow c$ background component (dot-dashed), total background (dotted) and the total fit result (solid).

We evaluate the following systematic errors in the fitting procedure. The width and the peak position of the signal Gaussian are varied by $\pm 1\sigma$, where σ is the error from the

$B \rightarrow D\pi$ calibration sample. For the continuum plus $b \rightarrow c$ background, we vary the ARGUS shape parameter by $\pm 1\sigma$, where σ is determined from the ΔE sideband data. The $B \rightarrow K^*\gamma$ component is varied by the branching fraction uncertainty. The other $b \rightarrow s\gamma$ component is varied by the uncertainty in the branching fraction [15] and the fraction to the $K\pi^+\pi^-\gamma$ final state [16]. For the charmless background, we vary the normalization by $\pm 100\%$. We take the sum in quadrature of all the deviations in the signal yield of these tests. The results are given in Table I.

TABLE I: Fitting systematic errors for $B^+ \rightarrow K^+\pi^+\pi^-\gamma$ and $B^0 \rightarrow K^0\pi^+\pi^-\gamma$.

	$B^+ \rightarrow K^+\pi^+\pi^-\gamma$	$B^0 \rightarrow K^0\pi^+\pi^-\gamma$
Signal M_{bc} parameters	(+0.65/−0.68)%	(+1.8/−2.2)%
Background ARGUS shape	(+2.4/−2.6)%	(+4.0/−4.5)%
$B \rightarrow K^*\gamma$	(+0.25/−0.11)%	(+0.01/−0.17)%
Other $b \rightarrow s\gamma$	(+0.36/−0.54)%	(+0.84/−0.96)%
Charmless background	(+0.60/−0.60)%	(+0.74/−0.74)%
MC stat. error	(+4.8/−4.8)%	(+11.5/−11.0)%
Total fitting error	(+5.5/−5.6)%	(+12.4/−12.1)%

In order to decompose intermediate resonances that may be involved in the $K^+\pi^+\pi^-$ final state, we perform an unbinned maximum likelihood fit to the M_{bc} and $M_{K\pi\pi}$ distributions of the $B^+ \rightarrow K^+\pi^+\pi^-\gamma$ candidates. We do not use $B^0 \rightarrow K^0\pi^+\pi^-\gamma$ due to the limited statistics. There are many possible resonances that can contribute: $K_1(1270)$, $K_1(1400)$, $K_2^*(1430)$, $K^*(1410)$, $K^*(1680)$, and so on. Here we consider the first three resonances, and include an additional non-resonant $B^+ \rightarrow K^+\pi^+\pi^-\gamma$ component whose $M_{K\pi\pi}$ distribution is modeled with a set of two broad Gaussian functions, which are determined from an inclusive $B \rightarrow X_s\gamma$ MC sample. The $B \rightarrow K_2^*(1430)\gamma$ component, which is already measured, is fixed in the fit. We model the $K_1(1270)$ resonance as a sum of three decay chains, $K_1(1270)^+ \rightarrow K^+\rho^0$, $\rho^0 \rightarrow \pi^+\pi^-$; $K_1(1270)^+ \rightarrow K^{*0}\pi^+$, $K^{*0} \rightarrow K^+\pi^-$; and $K_1(1270)^+ \rightarrow K_0^*(1430)\pi^+$, $K_0^*(1430) \rightarrow K^+\pi^-$. We do not consider interference between these final states. The $M_{K\pi\pi}$ distribution for each decay chain is described by convolving the two relativistic Breit-Wigner functions of the decay chain. The $K_1(1400)$ resonance is modeled with a single decay chain, $K_1(1400)^+ \rightarrow K^{*0}\pi^+$, $K^{*0} \rightarrow K^+\pi^-$. The $M_{K\pi\pi}$ distributions of other $b \rightarrow s\gamma$ and continuum plus $b \rightarrow c$ backgrounds are modeled by using a function $(p_0 + p_1x)e^{p_2+p_3x+p_4x^2}$, where $x = M_{K\pi\pi}$, and p_i ($i = 0 \dots 4$) are empirical parameters that are determined by using MC samples.

In order to enhance the $K_1(1270)$ component, we further select the events with the $\pi^+\pi^-$ mass in the ρ^0 mass region, $0.6 \text{ GeV}/c^2 < M_{\pi\pi} < 0.9 \text{ GeV}/c^2$ (the $K_1(1270) \rightarrow K\rho$ branching fraction $(42 \pm 6)\%$ being much larger than the $K_1(1400) \rightarrow K\rho$ branching fraction $(3 \pm 3)\%$). Even with this requirement, substantial $K^*\pi\gamma$ and $K_0^*(1430)\pi\gamma$ events remain in the sample due to the overlapping kinematics of the final states. The fit result is shown in Fig. 2. We find 102 ± 22 events for the $B^+ \rightarrow K_1(1270)^+\gamma$ component in the mass range $1 \text{ GeV}/c^2 < M_{K\pi\pi} < 2 \text{ GeV}/c^2$ with a statistical significance of 9.2σ . We find the $K_1(1400)\gamma$ contribution is much smaller than that from $K_1(1270)\gamma$, and is consistent with zero.

Similarly, we select the events with the $K^+\pi^-$ mass in the K^{*0} mass region, $0.8 \text{ GeV}/c^2 < M_{K\pi} < 1.0 \text{ GeV}/c^2$, in order to enhance the $K_1(1400)$ component (the $K_1(1400) \rightarrow K^*\pi$ branching fraction $(94 \pm 6)\%$ being much larger than the $K_1(1270) \rightarrow K^*\pi$ branching fraction

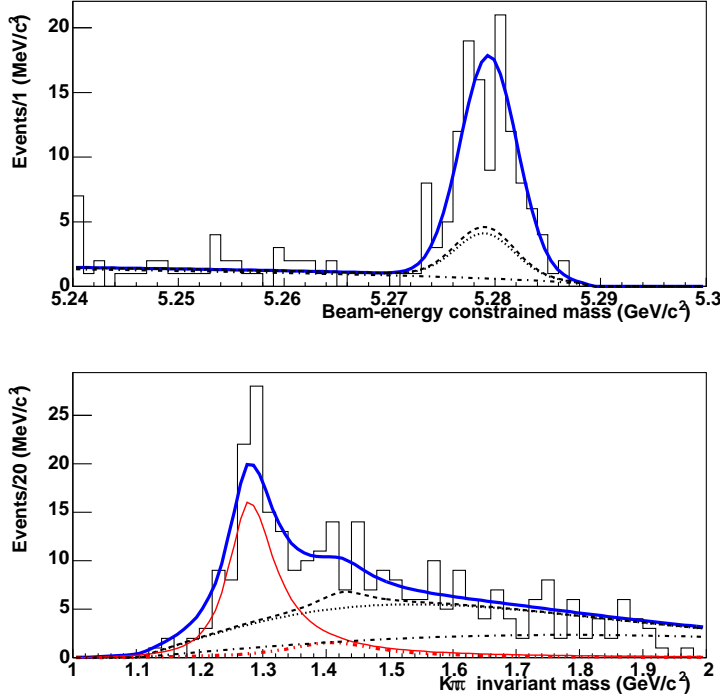


FIG. 2: M_{bc} distribution for $1.2 \text{ GeV}/c^2 < M_{K\pi\pi} < 1.4 \text{ GeV}/c^2$ (top) and $M_{K\pi\pi}$ distribution for $M_{bc} > 5.27 \text{ GeV}/c^2$ (bottom) of the $K_1(1270)\gamma$ enriched sample with $0.6 \text{ GeV}/c^2 < M_{\pi\pi} < 0.9 \text{ GeV}/c^2$. Lines show the projections of the fit results for the continuum plus $b \rightarrow c$ background component (dot-dashed), total background without and with the $K_2^*(1430)\gamma$ component (dotted and dashed, respectively), $K_1(1270)\gamma$ (thin solid line) and $K_1(1400)\gamma$ (dot-dot-dashed) components, and the sum of all components (thick solid line).

(16 ± 5)%). The fit result is shown in Fig. 3. We still find a sizable $K_1(1270)\gamma$ component, and only a small $K_1(1400)\gamma$ component. We find 23 ± 26 events for the $B^+ \rightarrow K_1(1400)^+\gamma$ component in the mass range $1 \text{ GeV}/c^2 < M_{K\pi\pi} < 2 \text{ GeV}/c^2$ with a statistical significance of 1.3σ . Since the $K_1(1400)\gamma$ component is not significant, we set a 90% confidence level upper limit on the signal yield, N_{90} , which is calculated from the relation $\int_0^{N_{90}} \mathcal{L}(n) dn = 0.9 \int_0^\infty \mathcal{L}(n) dn$, where $\mathcal{L}(n)$ is the likelihood function with the signal yield fixed at n .

Additional tests are performed to evaluate the fitting systematic errors, in addition to those previously mentioned. We vary the $K_1(1270)$ and $K_1(1400)$ signal peak positions and widths according to the errors given by the Particle Data Group (PDG) [17]. We vary the $K_2^*(1430)\gamma$ branching fraction according to the PDG error. These fitting systematic errors are summarized in Table II.

The reconstruction efficiency is obtained from the signal MC samples. For the inclusive measurement, we consider the efficiency difference between the different intermediate state assumptions; we use a weighted average of the $B^+ \rightarrow K^+\pi^+\pi^-\gamma$ efficiencies for non-resonant decays and the one through the $K_1(1270)^+$ state, using the measured ratio of the $K_1(1270)^+\gamma$ and non-resonant $K^+\pi^+\pi^-\gamma$ events ($K_1(1400)^+\gamma$ and $K_2^*(1430)^+\gamma$ events are neglected). We assume the same ratio for the $B^0 \rightarrow K^0\pi^+\pi^-\gamma$ efficiency. We estimate the systematic errors due to photon detection (2.8%), tracking ($\sim 1\%$ per track), charged particle identification (1–2% per particle), and K_S^0 reconstruction (4.5%) from control samples of radiative Bhabha

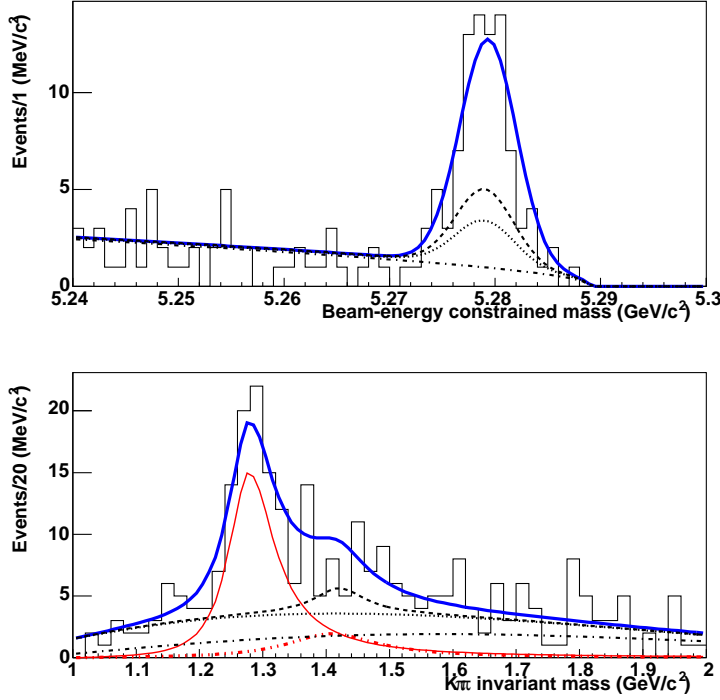


FIG. 3: M_{bc} distribution for $1.2 \text{ GeV}/c^2 < M_{K\pi\pi} < 1.4 \text{ GeV}/c^2$ (top) and $M_{K\pi\pi}$ distribution for $M_{bc} > 5.27 \text{ GeV}/c^2$ (bottom) of the $K_1(1400)\gamma$ enriched sample with $0.8 \text{ GeV}/c^2 < M_{K\pi} < 1.0 \text{ GeV}/c^2$. Lines show the projections of the fit results with the same definition as in Fig. 2.

events, partially reconstructed $D^{*+} \rightarrow D^0\pi^+$, $D^0 \rightarrow K_S^0\pi^+\pi^-$ events, D^{*+} -tagged $D^0 \rightarrow K^-\pi^+$ decays, and the ratio of $D^+ \rightarrow K_S^0\pi^+$ decays to $D^+ \rightarrow K^-\pi^+\pi^+$ decays, respectively. The systematic error due to the likelihood ratio and π^0/η veto requirements is estimated to be 6.1% (3.2%) from a control sample of $B^0 \rightarrow D^+\pi^-$, $D^+ \rightarrow K^-\pi^+\pi^+$ ($B^+ \rightarrow \bar{D}^0\pi^+$, $\bar{D}^0 \rightarrow K_S^0\pi^+\pi^-$) events for the $B^+ \rightarrow K^+\pi^+\pi^-\gamma$ ($B^0 \rightarrow K^0\pi^+\pi^-\gamma$) mode. The efficiencies and their systematic errors are summarized in Table III.

Using the signal yield and reconstruction efficiency for $B^+ \rightarrow K_1(1270)^+\gamma$, and the

TABLE II: Fitting systematic errors for $B^+ \rightarrow K_1(1270)^+\gamma$ and $B^+ \rightarrow K_1(1400)^+\gamma$.

	$B^+ \rightarrow K_1(1270)^+\gamma$	$B^+ \rightarrow K_1(1400)^+\gamma$
Signal M_{bc} parameters	(+0.35/−0.14)%	(+0.46/−0.50)%
Background ARGUS shape	(+0.33/−0.36)%	(+0.31/−0.32)%
$B \rightarrow K^*\gamma$	(+0.01/−0.02)%	(+0.63/−0.27)%
Other $b \rightarrow s\gamma$	(+0.03/−0.00)%	(+0.05/−0.07)%
Charmless background	(+0.01/−0.02)%	(+0.13/−0.13)%
Breit-Wigner line shape	(+0.95/−1.0)%	(+4.4/−5.1)%
$\mathcal{B}(B^+ \rightarrow K_2^*(1430)^+\gamma)$	(+0.60/−0.70)%	(+28.6/−28.6)%
MC stat. error	(+6.6/−6.4)%	(5.3/−5.2)%
Total fitting error	(+6.7/−6.5)%	(+29.4/−29.5)%

number of B meson pairs $((152.0 \pm 0.6) \times 10^6)$, we find

$$\mathcal{B}(B^+ \rightarrow K_1(1270)^+\gamma) = (4.28 \pm 0.94(\text{stat.}) \pm 0.43(\text{syst.})) \times 10^{-5}. \quad (3)$$

Similarly, we measure the inclusive branching fractions of $B^+ \rightarrow K^+\pi^+\pi^-\gamma$ and $B^0 \rightarrow K^0\pi^+\pi^-\gamma$ in the mass range $1 \text{ GeV}/c^2 < M_{K\pi\pi} < 2 \text{ GeV}/c^2$,

$$\begin{aligned} \mathcal{B}(B^+ \rightarrow K^+\pi^+\pi^-\gamma) &= (2.50 \pm 0.18 \pm 0.22) \times 10^{-5}, \\ \mathcal{B}(B^0 \rightarrow K^0\pi^+\pi^-\gamma) &= (2.43 \pm 0.36 \pm 0.34) \times 10^{-5}. \end{aligned} \quad (4)$$

For $B^+ \rightarrow K_1(1400)^+\gamma$, we use the upper limit on the signal yield to which the fitting systematic error is added, and the systematic error subtracted efficiency. We obtain an upper limit,

$$\mathcal{B}(B^+ \rightarrow K_1(1400)^+\gamma) < 1.44 \times 10^{-5} \quad (90\% \text{ C.L.}). \quad (5)$$

These results are summarized in Table IV.

We find the branching fraction for $B^+ \rightarrow K_1(1270)^+\gamma$ is larger than that for $B^+ \rightarrow K_1(1400)^+\gamma$. This difference may be explained by the $K_1(1270)$ – $K_1(1400)$ mixing angle [7], but the branching fraction for $B^+ \rightarrow K_1(1270)^+\gamma$ itself is much larger than theory predictions [6, 7]. Both results are consistent with previous upper limits [3]; the $B^+ \rightarrow K_1(1400)^+\gamma$ upper limit is significantly reduced.

The inclusive branching fraction $B^+ \rightarrow K^+\pi^+\pi^-\gamma$ is consistent with the previous measurement with a significantly improved error [3]. The neutral decay mode $B^0 \rightarrow K^0\pi^+\pi^-\gamma$ is measured to have a similar branching fraction, which suggests the yet to be measured $B^0 \rightarrow K_1(1270)^0\gamma$ branching fraction could also be large.

To conclude, we observe a new radiative decay mode, $B \rightarrow K_1(1270)\gamma$, with a branching fraction of $(4.28 \pm 0.94(\text{stat.}) \pm 0.43(\text{syst.})) \times 10^{-5}$. Although the corresponding neutral decay is not measured yet, we expect a similar branching fraction since we have also measured the inclusive branching fractions for $B^+ \rightarrow K^+\pi^+\pi^-\gamma$ and $B^0 \rightarrow K^0\pi^+\pi^-\gamma$ and found that they are close each other. With a larger data sample, these decay modes can be used to search for physics beyond the SM.

We would like to thank the KEKB group for the excellent operation of the accelerator, the KEK Cryogenics group for the efficient operation of the solenoid, and the KEK computer group and the National Institute of Informatics for valuable computing and Super-SINET network support. We acknowledge support from the Ministry of Education, Culture, Sports,

TABLE III: Relative systematic errors and total efficiencies.

	$B^+ \rightarrow K^+\pi^+\pi^-\gamma$			$B^0 \rightarrow K^0\pi^+\pi^-\gamma$
	$K_1(1270)^+\gamma$	$K_1(1400)^+\gamma$	inclusive	inclusive
Photon detection	$\pm 2.8\%$	$\pm 2.8\%$	$\pm 2.8\%$	$\pm 2.8\%$
Tracking	$\pm 3.0\%$	$\pm 3.0\%$	$\pm 3.0\%$	$\pm 2.1\%$
Particle id.	$\pm 2.1\%$	$\pm 2.1\%$	$\pm 2.1\%$	$\pm 1.0\%$
K_S^0 reconstruction	—	—	—	$\pm 2.4\%$
\mathcal{R}_S and π^0/η veto	$\pm 6.1\%$	$\pm 6.1\%$	$\pm 6.1\%$	$\pm 3.2\%$
Total efficiency error	$\pm 7.6\%$	$\pm 7.6\%$	$\pm 7.6\%$	$\pm 6.6\%$
Efficiency	$(1.56 \pm 0.12)\%$	$(2.68 \pm 0.20)\%$	$(8.36 \pm 0.64)\%$	$(1.82 \pm 0.12)\%$

TABLE IV: Results on the signal yields, efficiencies, branching fractions and significances.

	yield	efficiency	branching fraction	significance
$B^+ \rightarrow K_1(1270)^+\gamma$	102 ± 22	$(1.56 \pm 0.12)\%$	$(4.28 \pm 0.94 \pm 0.43) \times 10^{-5}$	9.2σ
$B^+ \rightarrow K_1(1400)^+\gamma$	23 ± 26	$(2.68 \pm 0.20)\%$	$< 1.44 \times 10^{-5}$	1.3σ
$B^+ \rightarrow K^+\pi^+\pi^-\gamma$	318 ± 22	$(8.36 \pm 0.64)\%$	$(2.50 \pm 0.18 \pm 0.22) \times 10^{-5}$	20.4σ
$B^0 \rightarrow K^0\pi^+\pi^-\gamma$	67 ± 10	$(1.82 \pm 0.12)\%$	$(2.43 \pm 0.36 \pm 0.34) \times 10^{-5}$	10.9σ

Science, and Technology of Japan and the Japan Society for the Promotion of Science; the Australian Research Council and the Australian Department of Education, Science and Training; the National Science Foundation of China under contract No. 10175071; the Department of Science and Technology of India; the BK21 program of the Ministry of Education of Korea and the CHEP SRC program of the Korea Science and Engineering Foundation; the Polish State Committee for Scientific Research under contract No. 2P03B 01324; the Ministry of Science and Technology of the Russian Federation; the Ministry of Education, Science and Sport of the Republic of Slovenia; the National Science Council and the Ministry of Education of Taiwan; and the U.S. Department of Energy.

* on leave from Nova Gorica Polytechnic, Nova Gorica

- [1] CLEO Collaboration, R. Ammar *et al.*, Phys. Rev. Lett. **71**, 674 (1993); CLEO Collaboration, T. E. Coan *et al.*, Phys. Rev. Lett. **84**, 5283 (2000); BaBar Collaboration, B. Aubert *et al.*, Phys. Rev. Lett. **88**, 101805 (2002); Belle Collaboration, M. Nakao *et al.*, Phys. Rev. D **69**, 112001 (2004).
- [2] We use K^* to denote $K^*(892)$ throughout the paper.
- [3] Belle Collaboration, S. Nishida *et al.*, Phys. Rev. Lett. **89**, 231801 (2002).
- [4] Throughout this paper, the inclusion of the charge conjugate mode decay is implied unless otherwise stated.
- [5] Belle Collaboration, A. Drutskoy *et al.*, Phys. Rev. Lett. **92**, 051801 (2004).
- [6] S. Veseli and M.G. Olsson, Phys. Lett. B **367**, 309 (1996); D. Ebert, R.N. Faustov, V.O. Galkin and H. Toki, Phys. Rev. D **64**, 054001 (2001); A. Safir, Eur. Phys. J. C **3**, 15 (2001).
- [7] H.Y. Cheng and C.K. Chua, Phys. Rev. D **69**, 094007 (2004).
- [8] M. Gronau, Y. Grossman, D. Pirjol and A. Ryd, Phys. Rev. Lett. **88**, 051802 (2002).
- [9] S. Kurokawa and E. Kikutani, Nucl. Instrum. Meth. A **499**, 1 (2003), and other papers includes in this volume.
- [10] Belle Collaboration, A. Abashian *et al.*, Nucl. Instrum. Meth. A **479**, 117 (2002).
- [11] R.A.Fisher, Annals of Eugenics **7**, 179 (1936).
- [12] Belle Collaboration, S.H. Lee *et al.*, Phys. Rev. Lett. **91**, 261801 (2003).
- [13] G. C. Fox and S. Wolfram, Phys. Rev. Lett. **41**, 1581 (1978).
- [14] ARGUS Collaboration, H. Albrecht *et al.*, Phys. Lett. B **229**, 304 (1989).
- [15] Heavy Flavor Averaging Group, <http://www.slac.stanford.edu/xorg/hfag>.
- [16] Belle Collaboration, S. Nishida *et al.*, Phys. Rev. Lett. **93**, 0318038 (2004).
- [17] Particle Data Group, S. Eidelman *et al.*, Phys. Lett. B **592**, 1 (2004).